ATLAS

A. Annovi, M. Antonelli(Resp.), M.M. Beretta, H. Bilokon,
E. Capitolo(Tech.), A. Castegnaro(Laur.), F. Cerutti, V. Chiarella, G. Corradi(Tech.), M. Curatolo,
R. Di Nardo(Ass. Ric.), M. Dreucci, B. Esposito, M. Gatta (Tech.), C. Gatti, P.F. Laurelli,
G. Maccarrone, A. Martini, G. Mancini(laur.), G. Nicoletti, G. Pileggi (Tech.),
B. Ponzio(Tech.), V. Russo(Tech.), A. Sansoni,V. Santini(laur.)
M. Testa, T. Vassilieva (Tech.), E. Vilucchi, G. Volpi.

In collaboration with:
Centro di Calcolo:
M. Pistoni, D. Spigone

1 Introduction

In the 2012 data taking ATLAS collected proton-proton collisions at 8 TeV center of mass energy corresponding to an integrated luminosity of about 20 fb^{-1}. On 4 July, 2012, the LHC experiments reported the evidence of the Higgs boson with a mass of about of 125 GeV. Our group contributed significantly to this discovery with fundamental contributions to the analysis $H \to ZZ \to 4\ell$, and $H \to WW \to 2\ell 2\nu$ as will be described in the following. In both channels we benefit of the matured expertize on performances. Missing Transverse Energy measurement is one of the main object used in the WW channel, and muon reconstruction (efficiency, momentum calibratio, etc) is crucial for the 4 lepton channel. These contributions have been made possible also thanks to the reliability and the innovative tools available on the LNF Tier2 that has been recently approved by the INFN. In parallel with the data taking activity, including shifts and maintenance, we are deeply involved in two upgrade Phase I activities the Fast TracK (FTK) for the upgrade of the trigger system, and the new Small Wheel for the upgrade of the muon system.

2 Reconstruction of the missing transverse energy

The reconstruction and calibration of the missing transverse energy ($\not{E}_T$) developed in ATLAS makes use of the full event reconstruction and of a calibration based on reconstructed physics objects (refined calibration) [1)]
Calorimeter cells are associated with a parent reconstructed and identified high-p_{T} object in a chosen order: electrons, photons, hadronically decaying τ-leptons, jets and muons.
Cells belonging to topologically formed clusters (topoclusters) not associated with any such objects are also taken into account in the $\not{E}_T$ calculation.
Once the cells are associated with a category of object as described above and calibrated accordingly, $\not{E}_T$ is calculated as follows:

$$E_{x(y)}^{\mathrm{miss,calo}} = E_{x(y)}^{\mathrm{miss},e} + E_{x(y)}^{\mathrm{miss},\gamma} + E_{x(y)}^{\mathrm{miss},\tau} + E_{x(y)}^{\mathrm{miss,jets}} + E_{x(y)}^{\mathrm{miss,softjets}} + E_{x(y)}^{\mathrm{miss,calo},\mu} + E_{x(y)}^{\mathrm{miss,CellOut}} \quad (1)$$

where each term is calculated from the negative sum of calibrated cell energies inside the corresponding objects:

- $E_{x(y)}^{\mathrm{miss},e}$, $E_{x(y)}^{\mathrm{miss},\gamma}$, $E_{x(y)}^{\mathrm{miss},\tau}$ are reconstructed from cells in electrons, photons and taus, respectively
- $E_{x(y)}^{\mathrm{miss,jets}}$ is reconstructed from cells in jets with $p_{\mathrm{T}} > 20$ GeV
- $E_{x(y)}^{\mathrm{miss,softjets}}$ is reconstructed from cells in jets with 7 GeV $< p_{\mathrm{T}} <$ 20 GeV
- $E_{x(y)}^{\mathrm{miss,calo},\mu}$ is the contribution to $\not{E}_T$ originating from the energy lost by muons in the calorimeter
- the $E_{x(y)}^{\mathrm{miss,CellOut}}$ term is calculated from the cells in topoclusters which are not included in the reconstructed objects. For the calculation of this term an energy flow algorithm is used.

The final $E_{x(y)}^{\mathrm{miss}}$ is then calculated adding the $E_{x(y)}^{\mathrm{miss},\mu}$ term.
The $\not{E}_T$ muon term is calculated from the momenta of muon tracks reconstructed with $|\eta| < 2.7$:
$E_{x(y)}^{\mathrm{miss},\mu} = -\sum_{\mathrm{selected\ muons}} p_{x(y)}^{\mu}$
In the region $|\eta| < 2.5$, only well reconstructed muons in the muon spectrometer with a matched track in the inner detector are considered.

In order to deal appropriately with the energy deposited by the muon in calorimeters, the muon term is calculated differently for isolated and non-isolated muons.
This algorithm, allowing to calibrate cells separately and independently according to the object to which they belong, has the best performances in terms of linearity and resolution of the $\not{E}_T$ for events containing electrons, photons, taus and muons.
The $\not{E}_T$ reconstruction, especially the low-pt contribution $E_{x(y)}^{\text{miss,CellOut}}$ and $E_{x(y)}^{\text{miss,softjets}}$, is strongly affected by the increasing of pile-up. For several analyses involving $\not{E}_T$ measurements is essential a precise modeling of pile-up in simulation. Moreover the systematic uncertainty due to the pile-up is an issue for several important analyses concerning Higgs searches (see Sec. 3.1). The systematic uncertainty induced by the pileup can be determined in situ by exploiting the

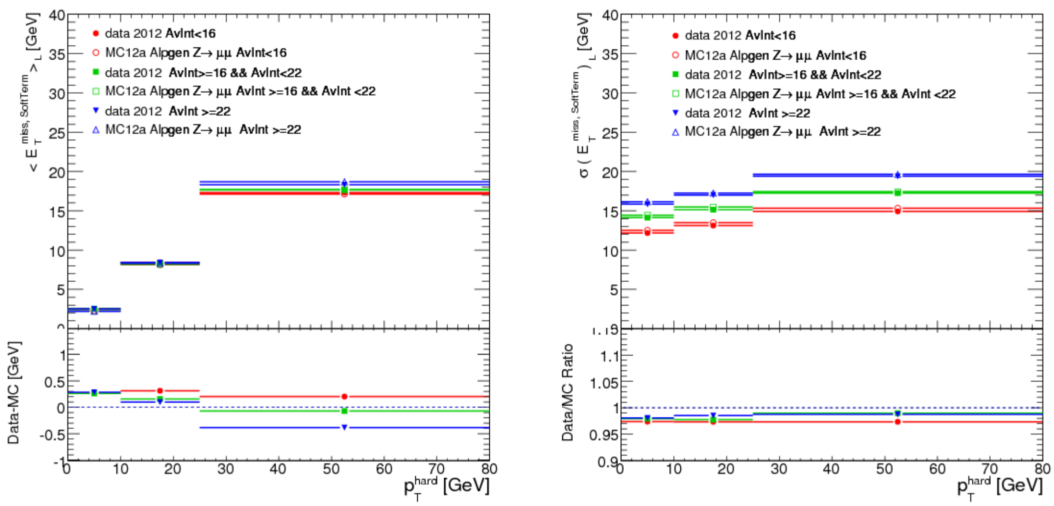

Figure 1: Mean (left) and resolution (right) of the longitudinal component of the soft-terms as a function of the total transverse momentum of the hard objects and the number of average bunch crossing interactions for data and MonteCarlo.

balance between the soft-terms and the total transverse momentum of the hard objects (p_T^{hard}) in $Z/\gamma^* \to \mu^+\mu^-$ events. In figure 1 the mean and the resolution of soft-terms as function of p_T^{hard} and the number of average bunch crossing interactions is shown.

3 PileUp suppression

In 2012, when about 30 mean interaction per bunch crossing are expected, pileup suppression will be an issue especially for the $\not{E}_T$ reconstruction. Degradation of $\not{E}_T$ performances are mostly due to the soft-terms contribution, $E_T^{\text{miss,CellOut}}$ and $E_T^{\text{miss,SoftJets}}$ term. Several techniques have been studied to reduce the impact of pile-up contribution, mainly combining the tracks pointing capability and the calorimeter information. The use of tracks pointing at the primary vertex allow to reduce the dependence on the $\not{E}_T$ performances the number of reconstructed vertices. However the acceptance of ATLAS tracking system is limited by $|\eta| < 2.5$ and further suppression is needed in forward region. Calorimeter clusters are used in the whole eta range to estimate the transverse energy density of the event ρ, following the approach for pile-up suppression in Ref. [2]. The energy density of the event ρ is an estimate of the in time and out of time pile-up activity and its contribution is subtracted to the $\not\!\!E_T$. The aim of the algorithm should ideally to improve resolution without affecting the linearity of the $\not\!\!E_T$. A trade-off between the two effects should be found. In Fig. 2(right) the $\not\!\!E_T$ resolution as a function of the number of vertices is shown for several methods. In Fig. 2(left) the effect on the calibration in $Z/\gamma^* \to \mu^+\mu^-$ events, is also shown. The best compromise is obtained when both tracks and calorimeter pile-up subtraction are used (green and magenta points). Black points correspond to the uncorrected $\not\!\!E_T$, red point and blue points correspond to algorithm using respectively tracks and clusters information alone.

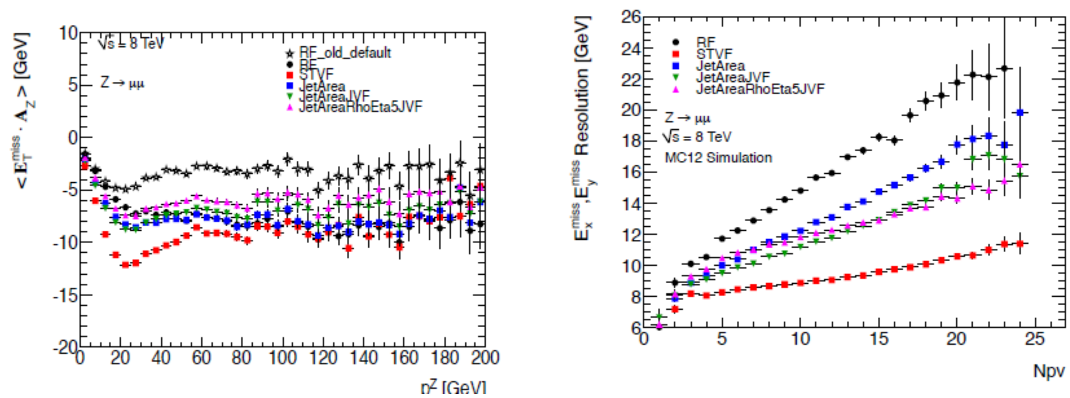

Figure 2: Left:$\not\!\!E_T$projection on the Z-boson p_T direction as a function of the p_T of the Z boson. Right: $\not\!\!E_{Tx}$ resolution as a function of the number of vertices in the event. Black points correspond to the uncorrected $\not\!\!E_T$, other colors correspond to several pile-up suppression algorithms.

3.1 Search for the Higgs boson in the $H \to WW^{(*)} \to l\nu l\nu$ decay channel

For a SM Higgs boson with a mass greater than 135 GeV, the $H \to WW^{(*)}$ is the dominant decay mode and in the region around m_H= 160 GeV the purely leptonic mode $H \to WW^{(*)} \to l\nu l\nu$ is the most sensitive channel. The experimental signature for this channel consists of two opposite sign, isolated and with high transverse momentum leptons (e or μ) and large missing transverse energy, $\not{E}_T$, due to the undetected neutrino. The main backgrounds for this channel, after the two leptons requirement, are the Drell-Yan and $Z + jets$ processes, tt and single top ($tW/tb/tqb$), WW , other diboson processes ($WZ/ZZ/W\gamma$), and $W + jets$ where a jet is misidentified as a lepton. The full 2011 and 2012 data sample have been used for this analysis [3] corresponding to an integrated luminosity of 4.6 fb^{-1}at a center of mass energy of 7 TeV and 21 fb^{-1}at 8 TeV, respectively. Data are subdivided into $H +$ 0-jet, $H +$ 1-jet, and $H +$ 2-jet channel in order to maximize the sensitivity by applying further selection criteria that depend on the jet multiplicity. The event are selected by using a single lepton trigger requiring a high-p_T electron or muon. The selection criteria for this analysis are the following:

- exactly two isolated opposite-sign leptons (p_T> 25,15 GeV). This requirement reduces mostly the QCD and the $W + jets$ backgrounds.
- large missing energy requirement and Z mass veto cut, used to suppress the Drell-Yan and the $Z + jets$ contamination. In particular the quantity $E^{\rm miss}_{\rm T,rel}$ is used in this analysis defined as $E^{\rm miss}_{\rm T,rel}$= $\not{E}_T$ sin($\Delta\phi_{min}$) with $\Delta\phi_{min}$ = min ($\Delta\phi, \pi/2$) and $\Delta\phi$ defined as the absolute azimuthal angular difference between the $\not{E}_T$ vector and the nearest candidate lepton or jet with p_T> 25 GeV.
- b-jet veto is used to suppress the tt background.
- topological cuts ($\Delta\phi_{ll}$ <1.8 and m_{ll} <50 GeV) are used to reduce the SM WW contamination exploiting the spin correlations in the $WW^{(*)}$ system arising from the spin-0 nature of the Higgs boson.
- cuts on p_T^{ll} (0-jet channel) or p_T^{tot} [1] (1-jet and 2-jet channel) are used to further suppress Drell-Yan and soft-jets backgrounds.

---

[1]defined as the magnitude of the vector $\overrightarrow{p_T^{tot}}$ where $\overrightarrow{p_T^{tot}}$ is the vector sum of the transverse

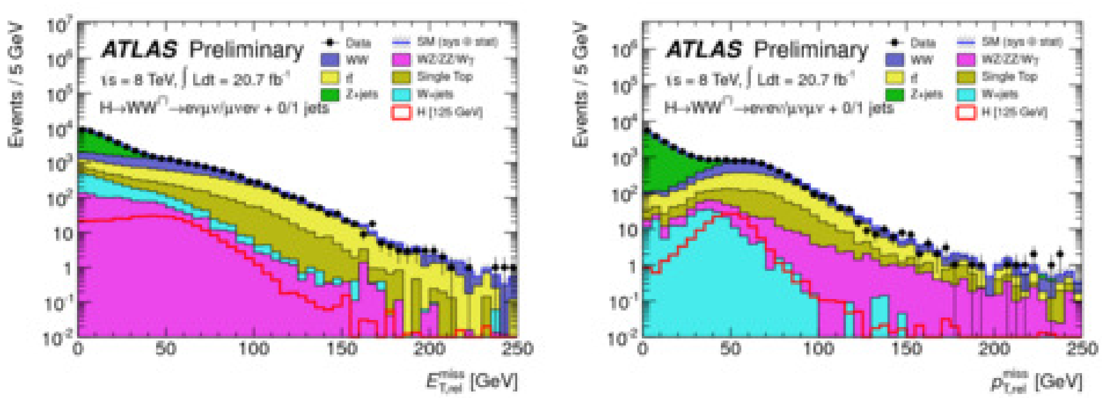

Figure 3: The $E^{\rm miss}_{\rm T,rel}$ distribution in the *emumue* channel (right) with the minimum lepton p_T cut applied and the $p_T^m iss$ distribution after the $E^{\rm miss}_{\rm T,rel}$ cut. The signal is shown for m_H= 125 GeV.

The crucial aspects for this analysis are

- the understanding of the $\not\!\!E_T$(real or fake). In fact $\not\!\!E_T$ spectrum and resolution are very sensitive to pile-up and with an higher pileup environment an increase of resolution is expected with the results that one have to tighten the cut on $E_{\mathrm{T,rel}}^{\mathrm{miss}}$ with a signal loss. Understanding of sources on data-MC disagreement on $\not\!\!E_T$ distribution (especially with high pileup) and improvements in additional Drell- Yan suppression are fundamental for this channel, in particular for the same-flavour channels. Figure 3(a) shows the $E_{\mathrm{T,rel}}^{\mathrm{miss}}$ distribution of the $e\mu$ and μe channel (left) and μe channel (right) with the minimum lepton p_{T} cut applied. and with the signal that is shown for $\mathrm{m_H}$= 125 GeV. In the same-flavour channels additional variable are used to further reject Drell- Yan background. An alternative measurement of the missing transverse momentum is obtained using inner detector tracks (p_T^{miss}). The resolution of this track-based quantity is less sensitive to pile-up interactions than the calorimeter-based $\not\!\!E_T$. Figure 3(b) shows the p_T^{miss} distribution after the pre-selection and the requirement on $E_{\mathrm{T,rel}}^{\mathrm{miss}}$.

- an excellent understanding of the background in the signal region. Signal free control region are used in data to constrain MC expectations in order to use MC simulation to extrapolate to the signal region. The $W + jets$ background contribution has been estimated using a control sample of events from data where one of the two leptons satisfies the identification and isolation criteria and the other lepton fails these criteria while satisfying a loosened selection. The $Z + jets$ background is normalized using a Z control sample ($|m_{ll} - M_Z| < 15$ GeV) correcting for mismodeling of $\not\!\!E_T$ tails. The top background prediction is normalized to the data using a control sample defined by reversing the b-jet veto and removing the requirements on m_{ll} and $\Delta\phi_{ll}$. The SM WW background, which represent the 65% of the total background, is normalized using an high-m_{ll} control region. The remaining backgrounds from di-bosons are estimated using MC simulation.

The transverse mass variable, m_{T}, is used in this analysis to test for the presence of a signal. This variable is defined as:

$$m_{\mathrm{T}} = \sqrt{(E_{\mathrm{T}}^{\mathrm{ll}} + E_{\mathrm{T}}^{\mathrm{miss}})^2 - |\mathbf{p}_T^{ll} + \mathbf{p}_T^{miss}|} \tag{2}$$

Figure 4 shows the distributions of the transverse mass for events satisfying all criteria in the $H + 0$-jet (left) and $H + 1$-jet (right) analyses at 8 TeV with a superimposed signal shown for $\mathrm{m_H}$= 125 GeV.

Njet	Signal	Total bkg.	Observed
=0	25 ± 5	161 ± 11	154
=1	7 ± 2	47 ± 6	62
>=2	1.2 ± 0.2	4.6 ± 0.7	2

Table 1: Summary table for 7 TeV. The observed numbers of events and the expected number of signal ($m_H = 125$ GeV) and background events are reported. The $e\mu + \mu e$ and $ee\mu\mu$ channels are combined.

Tables 1 and 2 show the expected numbers of signal ($m_H = 125$ GeV) and observed events at 7 TeV and 8 TeV respectively, for the N_{jet}=0, N_{jet}=0 and N_{jet}=2 analyses.
The expected and observed significances, shown in Figure 5a, at $m_H = 125GeV$ are 3.7 s.d.($p_0 = 1 \times 10^{-4}$) and 3.8 (8×10^{-5}) respectively. Figure 5b shows, as a function of $\mathrm{m_H}$, the

momenta of the jet, the two leptons and the $\not\!\!E_T$ vector

Njet	Signal	Total bkg.	Observed
=0	97 ± 20	739 ± 47	831
=1	40 ± 13	261 ± 30	309
>=2	8.7 ± 14	36 ± 4	55

Table 2: Summary table for 8 TeV. The observed numbers of events and the expected number of signal ($m_H = 125$ GeV) and background events are reported. The $e\mu + \mu e$ and $ee\mu\mu$ channels are combined.

observed and expected cross section upper limits at 95% CL, for the combined $H + 0$-jet, $H + 1$-jet and $H + 2$-jet analyses. Observed exclusion is for $m_H > 133$ GeV. The excess of events is quantified by the signal strength, which is defined as the ratio of the observed cross section to the value predicted for a Standard Model Higgs boson . For $m_H = 125$ GeV it is measured to be:

$$\mu = 1.03^{+0.22}_{-0.21}(stat)^{+0.21}_{-0.17}(theo.syst.)^{+0.11}_{-0.10}(expt.syst.)^{+0.05}_{-0.04}(lumi)$$

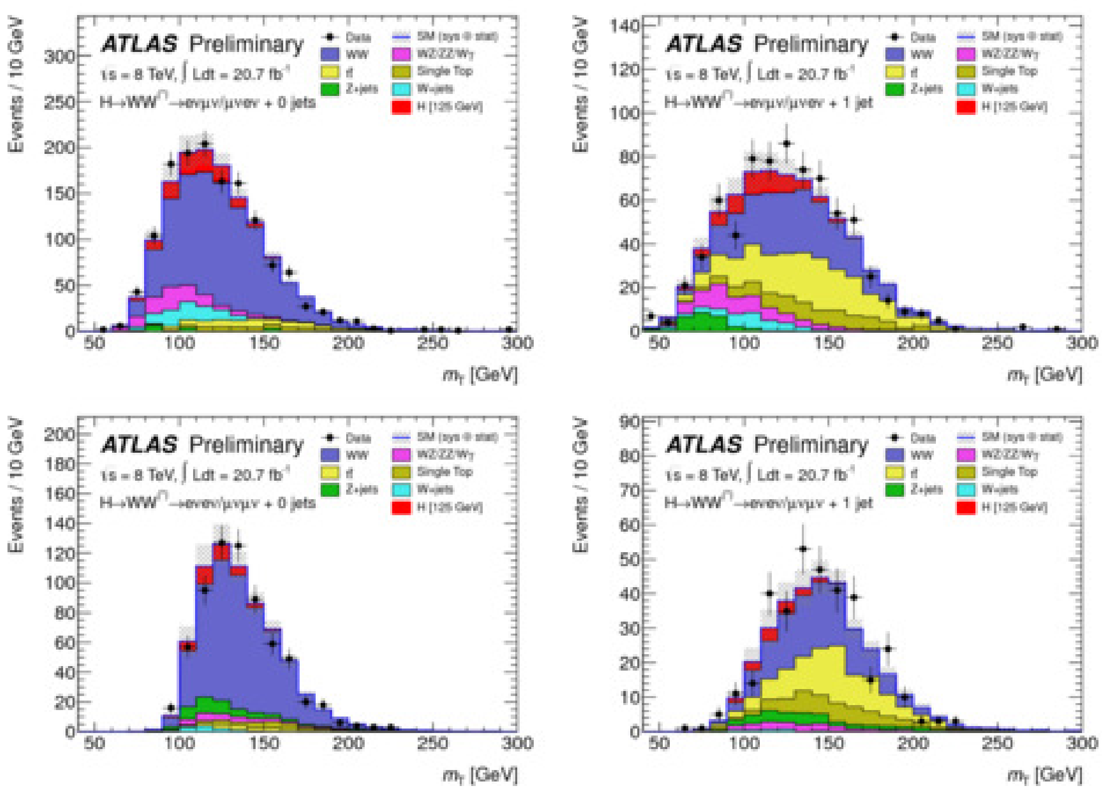

Figure 4: Transverse mass after all selection criteria in the $H + 0 - jet$ (left) and $H + 1 - jet$ (right) analyses at 8 TeV for opposite flavour (top) and same flavour (bottom) final state. The superimposed signal shown is for mH = 125 GeV.

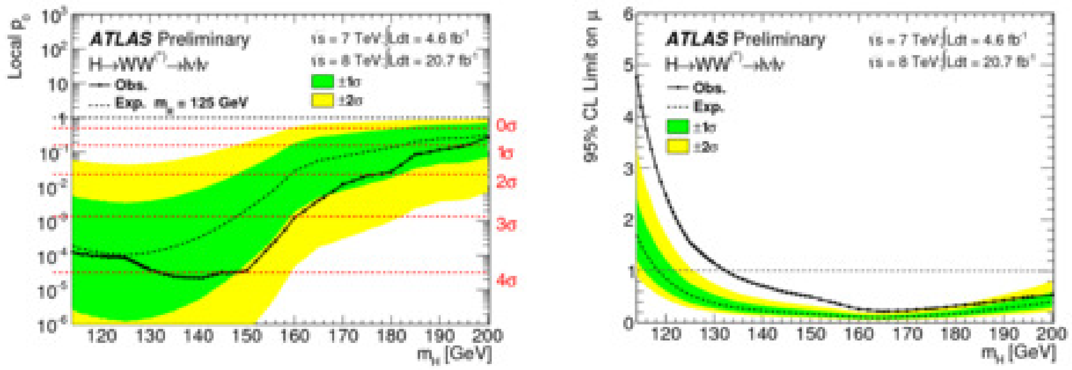

Figure 5: Results of p_0 and 95% C.L. upper limits using combined 7 TeV and 8 TeV data. The p_0 is given probability for the background-only scenario as a function of m_H. The expected 95% CL upper limit is computed in absence of the signal. For both figures, the smaller green bands re[resent $\pm 1\sigma$ uncertainties on the expected values, and the larger yellow badn represent $\pm 2\sigma$ uncertainties.

3.2 Observation of an excess of events in the search for the Standard Model Higgs boson in the $H \to ZZ^{(*)} \to 4l$ channel

The $H \to ZZ^{(*)} \to l^+l^-l'^+l'^-$ with l, l'=e or μ decay channel provide a good sensitivity for the SM Higgs boson search over a wide mass range. The main advantages for this channel are the purity (S/B$\sim$1) and the possibility to fully reconstruct the invariant mass of the Higgs boson. In particular three finale state (4μ, $4e$, $2e2\mu$) are considered. The latest results on this analysis uses all the data collected in 2011 corresponding to an integrated luminosity of 4.8 fb^{-1}at $\sqrt{s} = 7$ TeV and 21 fb^{-1}of data collected in 2012 at $\sqrt{s} = 8$ TeV.

The analysis searches for Higgs boson candidates is performed by selecting two same-avour, opposite-sign lepton pairs in an event. The impact parameter of each lepton along the beam axis is required to be within 10 mm of the reconstructed primary vertex. To reject cosmic rays, muon tracks are required to have a transverse impact parameter less than 1 mm. Each muon (electron) must satisfy $p_{\mathrm{T}}>$ 6 GeV ($p_{\mathrm{T}}>$ 7 GeV) and be measured in the pseudorapidity range $|\eta| < 2.7$ ($|\eta| < 2.7$). The highest p_{T}lepton in the quadruplet must satisfy $p_{\mathrm{T}}>$ 20 GeV, and the second (third) lepton in p_{T}order must satisfy $p_{\mathrm{T}}>$ 15 GeV ($p_{\mathrm{T}}>$ 10 GeV). The leptons are required to be separated from each other by $\Delta R > 0.1$ if they are of the same avour and $\Delta R > 0.2$ otherwise. Only quadruplets with the same-flavour and opposite-sign lepton pair closest to the Z boson mass are kept. The pair with the mass closest to the Z boson mass is referred to as the leading di-lepton and its invariant mass, m_{12}, is required to be between 50 and 106 GeV. The remaining same-flavour, opposite-sign lepton pair is the sub-leading di-lepton and its invariant mass, m_{34}, is required to be in the range $m_{\mathrm{min}} < m_{34} < 115\,\mathrm{GeV}$, where m_{min} is $12\,\mathrm{GeV}$ for $m_{4\ell} < 140\,\mathrm{GeV}$ and rises linearly to $50\,\mathrm{GeV}$ at $m_{4\ell} = 190\,\mathrm{GeV}$. It stays at $50\,\mathrm{GeV}$ for $m_{4\ell} > 190\,\mathrm{GeV}$. The Z boson corresponding to the leading (sub-leading) di-lepton pair is labelled Z_1 (Z_2).

The $Z +$jets and $t\bar{t}$ background contributions are further reduced by applying impact parameter as well as track- and calorimeter-based isolation requirements on the leptons.

Main backgrounds to the $H \to ZZ^{(*)} \to 4l$ analysis are: the irreducible ZZ background and the reducible $Z +$jets and $t\bar{t}$ backgrounds. The former is estimated using MC simulation normalised to the theoretical cross section, while the latters are evaluated using data-driven methods. The composition of the reducible backgrounds depends on the avour of the sub-leading di-lepton and different approaches are taken for the $\ell\ell + \mu\mu$ and the $\ell\ell + ee$ final states. The expected $m_{4\ell}$

distributions for the total background and one signal hypothesis are compared to the combined $\sqrt{s} = 8$ TeV and $\sqrt{s} = 7$ TeV data in Fig. 6(a) for the mass range $80 - 170$ GeV. Figure 6(b) shows the distribution of the m_{34} versus the m_{12} invariant mass for the selected candidates in the $m_{4\ell}$ range $120 - 130$ GeV. The expected distributions for a SM Higgs boson with $m_H = 125$ GeV (the sizes of the boxes indicate the relative density) and for the total background (the intensity of the shading indicates the relative density) are also shown.

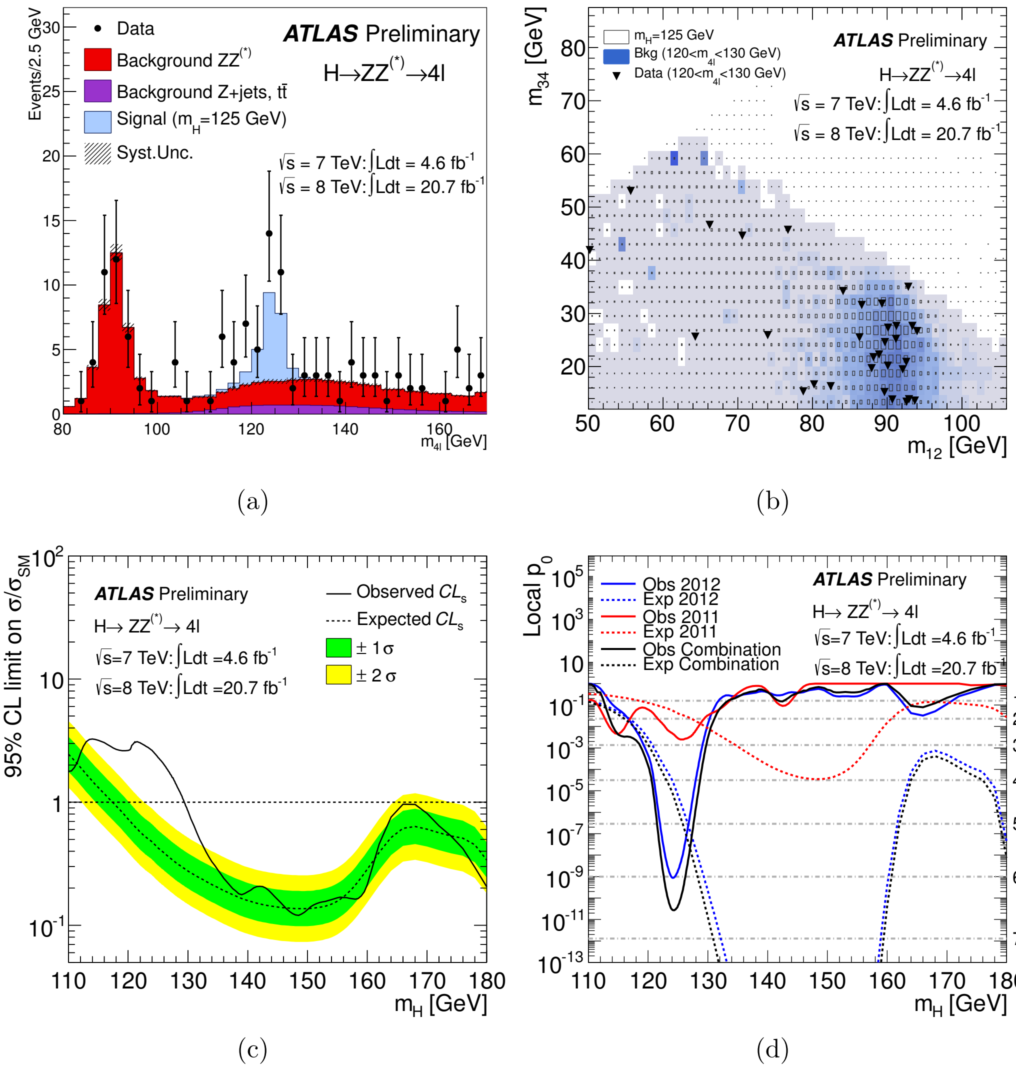

Figure 6: (a) The distribution of the four-lepton invariant mass, $m_{4\ell}$, for the selected candidates compared to the background expectation for the combined $\sqrt{s} = 8$ TeV and $\sqrt{s} = 7$ TeV data sets in the low mass range $80 - 170$ GeV. The signal expectation for the m_H=125 GeV hypothesis is also shown. (b) Distribution of the m_{34} versus the m_{12} invariant mass for the selected candidates in the $m_{4\ell}$ range 120-130 GeV. The expected distributions for a SM Higgs with $m_H = 125$ GeV (the sizes of the boxes indicate the relative density) and for the total background (the intensity of the shading indicates the relative density) are also shown. (c) The expected (dashed) and observed (full line) 95% CL upper limits on the SM Higgs boson production cross section as a function of m_H, divided by the expected SM Higgs boson cross section. The green and yellow bands indicate the expected limits with $\pm$ 1σ and $\pm$ 2σ fluctuations. (d) The observed local p0 for the combination of the 2011 and 2012 data sets (solid black line); the $\sqrt{s} = 7$ TeV and $\sqrt{s} = 8$ TeV data results are shown in solid lines (blue and red). The dashed curves show the expected median local p0 for the signal hypothesis when tested at the corresponding m_H.

Figure 6(c) shows the observed and expected 95% CL cross section upper limits, as a function of

m_H. The observed exclusion starts only at around 130 GeV due the excess at 125 GeV.
The significance of an excess is given by the probability, p_0, that a background-only experiment is more signal-like in terms of the test statistic than the observed data. In Fig. 6(d) the local p_0 is presented as a function of the m_H hypothesis.
The value for the tted mass from the prole likelihood is $mH = 124.3^{+0.6}_{-0.5}$ (stat) $^{+0.5}_{-0.3}$ (syst) GeV, where the systematic uncertainty is dominated by the energy and momentum scale uncertainties. The global signal strength factor μ [2] fitted at the best for m_H (124.3 GeV) is $1.7^{+0.5}_{-0.4}$.

3.3 Measurements of spin-parity properties of the new Higgs-like particle in the $H \to ZZ^{(*)} \to 4l$ decay channel

In order to confirm that the new discovered Higgs-like particle decaying in the $H \to ZZ^{(*)} \to 4l$ channel is the SM Higgs boson, the measurement of its spin and parity is needed since in the Standard Model the J^{CP} of the Higgs boson is predicted to be 0^{++}. The observation of the $\gamma\gamma$ decay of the new particle disfavour the spin 1 state[3]. The data used for this study correspond to 4.6 fb^{-1} at *sqrts* =7 TeV and 21 fb^{-1} at $\sqrt{s}$ =8 TeV using $H \to ZZ^{(*)} \to 4l$ candidates reconstructed in the region 115 GeV $< m_{4l} <$ 130 GeV. For the $X \to ZZ^{(*)} \to 4l$ decays, the sensitive observables to the spin and paity of the X particle are the masses of the two Z bosons and the five angles (a production angle and four decay angles) illustrated in Fig. 7 and defined as:

- $\theta_1(\theta_2)$: angle between the negative final state lepton and the direction of flight of Z_1 (Z_2) in the Z rest frame;
- Φ: angle between the decay planes of the four nal state leptons expressed in the four lepton rest frame;
- Φ_1: angle between the decay plane of the leading lepton pair and a plane dened by the vector of the Z_1 in the four lepton rest frame and the positive direction of the parton axis.
- θ^*: production angle of Z_1 in the 4-lepton rest frame.

These variables are evaluated for candidates passing the $H \to ZZ^{(*)} \to 4l$ selection described in 3.2 Four different spin-parity (J^P) states have been considered: 0^+, 0^-, 1^+, 1^-, 2^+ (equivalent to a Kaluza Klein graviton) , 2^- (pseudo-tensor), The analysis performed treats the spin/parity hypotheses pairwise in order to try to exclude one against the other. The distribution of the discriminating variables comparing 0^+ to 0^- for fully simulated JHU MC events after reconstruction and analysis selection are shown in figure 8. In order to distinguish different pairs of spin-parity, two multivariate approaches have been developed: one uses boosted decision tree (BDT) trained using the discriminating variables of fully simulated signal samples for each spin parity pair; the other uses a matrix element likelihood ratio (MELA) as a discriminant of different spin-parity hypotheses. Figure 9 shows the distributions of BDT and $\mathrm{J^P}-$MELA discriminannts compareing the The statistical test for a pair of J^P hypotheses is given by

$$\begin{aligned}\mathcal{P}^{ij} &= \mu^{\rm sig} f_i^{\rm sig} N_{\rm sig}\left[(1-\varepsilon)\cdot \mathrm{PDF}^{ij}_{\mathrm{H_0}} + \varepsilon \cdot \mathrm{PDF}^{ij}_{\mathrm{H_1}}\right] \\ &+ \sum_{\mathrm{bkg_k}} f_i^{\mathrm{bkg_k}} N_{\mathrm{bkg_k}} \mathrm{PDF}^{\mathrm{ij}}_{\mathrm{bkg_k}}, \end{aligned} \tag{3}$$

[2]The signal strenght μ acts as a scale factor on the total number of events predicted by the Standard Model for each of the Higgs boson signal processes

[3]Landau-Yang theorem

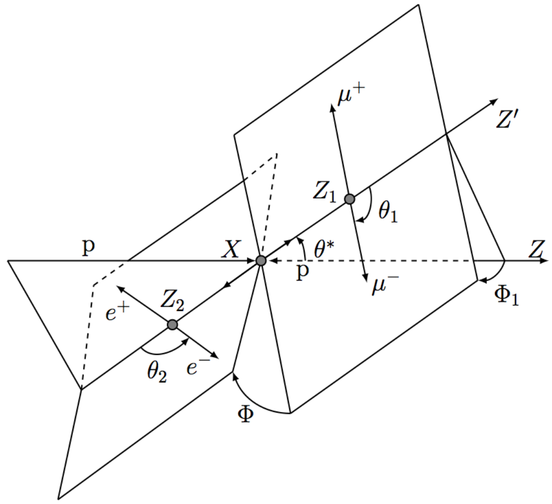

Figure 7: Production and decay angles for a $H \to ZZ^{(*)} \to 4l$ decay.

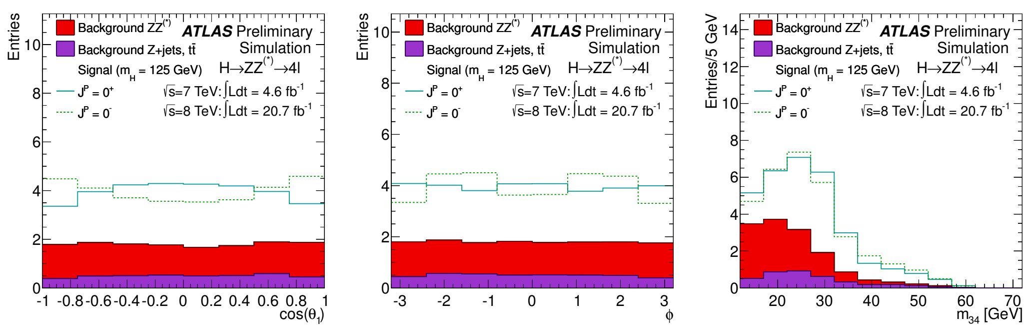

Figure 8: Expected distributions for $\sqrt{s} = 7$ TeV and $\sqrt{s} = 8$ TeV for $m_H = 125$ GeV including backgrounds in the mass range 115 GeV $< m_{4l} <$ 130 GeV comparing 0^+ versus 0^-.From left to right: $cos(\theta_1)$, ϕ, m_{34}.

where $\mu^{\rm sig}$ is the signal strength, $N_{\rm sig}$ is the number of expected SM signal events in the full mass region (115 GeV $< m_{4\ell} <$130 GeV), $f_i^{\rm sig}$ is the signal fraction in the $i^{\rm th}$ S/B mass bin (low and high), and $(1-\varepsilon)$ is the fraction of the $\rm H_0$ signal hypothesis represented by the $\mathrm{PDF}^{ij}_{\mathrm{H}_0}$ for the $j^{\rm th}$ $\rm J^P$ discriminant. Similarly, $f_i^{\rm bkg_k}$, $N_{\rm bkg_k}$ and $\rm PDF^{ij}_{bkg_k}$ are the bin fraction, total background and PDF for the $k^{\rm th}$ background, respectively. The parameters $N_{\rm sig}$, $N_{\rm bkg_k}$ are nuisance parameters which are constrained by Gaussian terms, and their uncertainties are determined from the nominal analysis. The parameter $\mu^{\rm sig}$ is left free in the fit.
Distributions of the log-likelihood ratio generated with more than 800,000 Monte Carlo pseudo-experiments when assuming the spin 0^+ hypothesis and testing the 0^-, 1+ and 2+ hypotheses for BDT analysis are shown in Fig. 10. The SM spin and parity remain the favoured hypothesis over the 0^-, 1^+ and 2^+ states. The 0^- is excluded at the 97.8% confidence level using $\rm CL_S$ when compared to 0^+ for the BDT analysis.

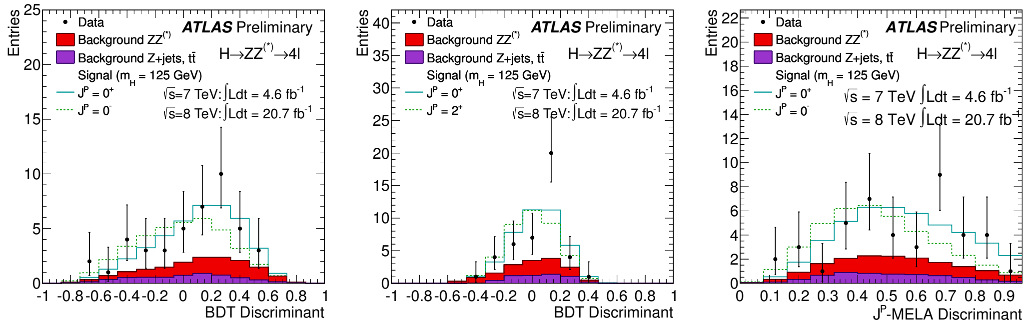

Figure 9: Distributions of the BDT (left and center) and $\mathrm{J^P}$−MELA (right) discriminants for data and MC expectations for the combined $\sqrt{s} = 7$ TeV and $\sqrt{s} = 8$ TeV data sets. For BDT analysis 0^+ vs 0^- and 0^+ vs 2^+ ; for $\mathrm{J^P}$−MELA 0^+ vs 0^- is shown.

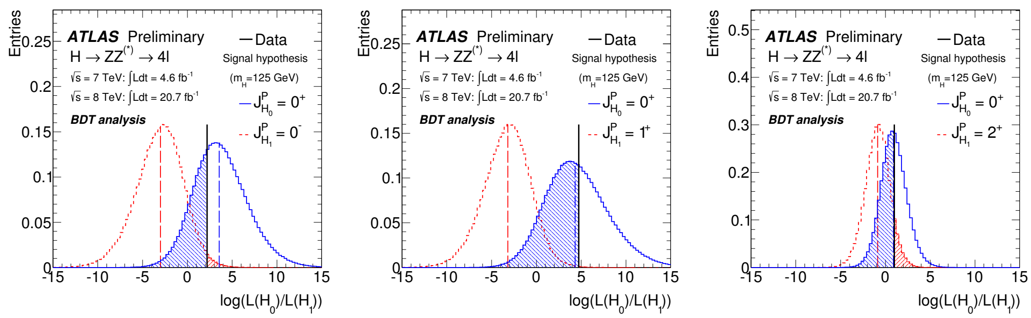

Figure 10: Log-likelihood ratio when assuming the spin 0^+ hypothesis and testing the 0^- (left), 1+ (center) and 2+ (right). The data are indicated by the solid vertical lines, and the median of each of the expected distributions is indicated by a dashed line. The shaded areas correspond to the observed p-values, representing the compatibility with the tested hypothesis H1 (right shaded area) and the assumed hypothesis H0 (left shaded area).

4 Tier-2

During the year 2012 the Frascati's Tier-2 successfully and continuously performed all the typical activities of an ATLAS Tier-2: Monte Carlo production and users and physics groups analysis, [4]. With the exception of the last two weeks of December when the site was shut down for the infrastructure works of the conditioning system, LNF Tier-2 has worked continuously, as we can see from the chart fig.11 left,

which highlights the different activities performed in the Tier-2 in 2012. Moreover, the efficiency of the site was always maintained above 90%, so it received the greatest share of data consistent with its size. Fugure 11 right reports the overall wall clock consumptions of all jobs at Frascati Tier-2, while the number of all jobs run at Frascati Tier-2 is reported in figure 12 left, finally, with the pie chart **??** right we can compare the CPU utilization of all jobs in the Italian ATLAS Tier-2 and see that for Frascati are consistent with the smaller size with respect to the other Tier-2s. Among the most significant activities involving Tier-2's staff, we can mention the operating system upgrade of the entire storage system and the migration of the farm from the gLite middleware to the new European Middleware Interface (EMI). Moreover, Frascati's Tier-2 hosts

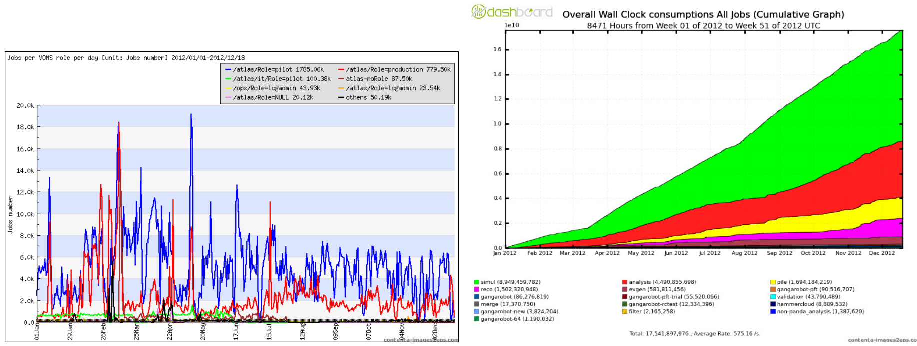

Figure 11: left: Activities performed at LNF tier-2 during year Tier-2; right:Wall clock time of all jobs at Frascati's Tier-2 in 2012

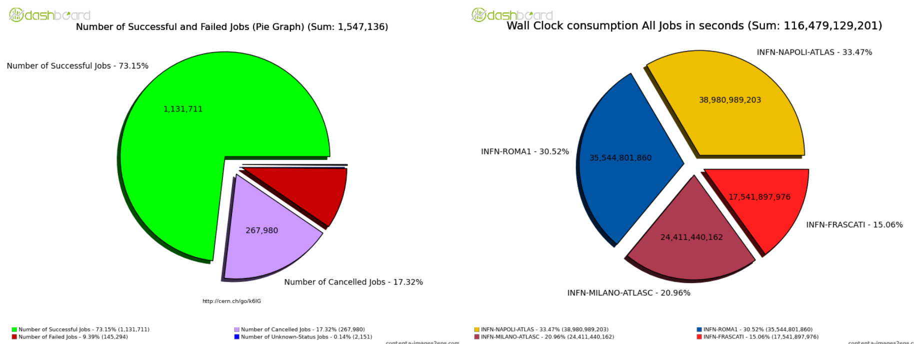

Figure 12: left: Jobs run at Frascati's Tier-2 in 2012; right: Wall clock time of all jobs at Italian Tier-2 in 2012.

a second DPM storage system to test new functionalities before to run them in production. About analysis activity, in collaboration with CERN developers, we promoted the use of Proof on Demand (PoD) [5)] for the analysis on ATLAS Tier-2s. PoD is a set of tools designed to interact with any resource management system (RMS) to start the PROOF daemons, then it is able to enable a PROOF cluster on the Tier-2's cluster. In this way any user can quickly setup its own PROOF cluster on the resources, with the RMS taking care of scheduling, priorities and accounting. PoD features an abstract interface to RMSs and provides several plugins for the most common RMSs: we experienced PROOF for data analysis on the on the Italian ATLAS Tier-2s: Frascati, Napoli and Roma1, for our tests we used both the gLite and PBS plug-ins and data were accessed via xrootd. So we provided the Tier-2 SRM, Disk Pool Manager, of xrootd protocol too. Thanks to the xrootd protocol, in the 2013 Frascati's Tier-2 will be part of the new ATLAS storage federation. In 13 left we show the results of submission tests we made on the Frascati Tier-2, where the number of allocated slots are in function of time for each bulk submission. In 13 right we report the results of the readout rate tests made at Roma1, Frascati and Napoli Tier-2's.

5 The Fast TracK Upgrade

The trigger is a fundamental part of any experiment at hadron colliders. It is needed to select on-line the interesting low cross-section physics from the huge QCD background.

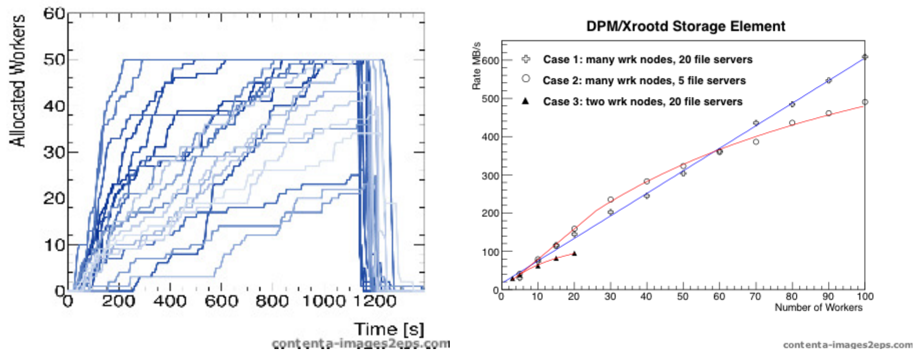

Figure 13: left: Results of the submission tests on the Frascati Tier-2: number of allocated slots as function of time for each bulk submission; right:Results of the readout rate tests at Roma1, Frascati and Napoli Tier-2's

Experience at high luminosity hadron collider experiments shows that controlling trigger rates at high instantaneous luminosity can be extremely challenging. As the luminosity increases, physics goals change in response to new discoveries, and detector aging. It is thus essential that the trigger system be flexible and robust, and redundant and significant operating margin. Providing high quality track reconstruction over the full ATLAS Inner Detector by the start of processing in the level-2 computer farm can be an important element in achieving these goals.
With the goal to improve and make more robust the ATLAS trigger, during summer 2007 the group joined the Fast-Track (FTK) proposal for "A hardware track finder for the ATLAS trigger". This is a proposal to build a hardware track finder as an upgrade to the ATLAS trigger. It will provide global reconstruction of tracks above 1 GeV/c in the silicon detectors, with high quality helix parameters, by the beginning of level-2 trigger processing. FTK can be particularly important for the selection of 3rd-generation fermions (b and τ). These have enormous background from QCD jets, which can be quickly rejected in level-2 if reconstructed tracks are available early. This R&D proposal was completed with the submission of the FTK Technical Proposal that was finally approved by the ATLAS collaboration meeting in June 2011. We are continuing the design and prototyping R&D aiming to prepare the FastTrack Technical Design Report to be submitted in Spring 2013.
The FTK processor performs pattern recognition with a custom device called the Associative Memory (AM). It is an array of VLSI chips that stores pre-calculated trajectories for a ultra-fast comparison with data. The first way to reduce the combinatorial at high luminosity is to work with better resolution in the AM. In order to do that, we will need a new AM chip with a high density of patterns, so that all possible tracks with a thinner resolution can be stored in the AM. Even with better resolution the number of candidate tracks that the AM will find at these high instantaneous luminosities will be very large. For this reason we redesigned the FTK architecture to increase the internal parallelism and data-flow to accommodate a larger flux of data.
For this purpose it was essential a new ideas. The efficiency curves for patterns is slowly increasing for efficiencies above 70%. This is due to the fact that many low probability patterns are needed to gain the missing efficiency. This is a consequence of the fact that the AM performs pattern recognition with a fixed resolution. We developed the idea of variable resolution patterns that increases the equivalent number of pattern per AMchip by a factor 3-5 with a corresponding reduction in hardware size [doi:10.1109/ANIMMA.2011.6172856].
In 2012 we completed the design of the new AMchip04 that for the first time implements the Associative Memory with variable resolution. This is a very challenging task because we need to

increase the pattern per chip with respect to the current AM chip designed for the SVT upgrade at CDF by a factor 30 with similar power consumption running at 100 MHz clock speed instead of 40 MHz. In order to achieve these goals we need several separate improvements: better technology 65 nm instead of 180 nm, design full custom cell that implements the core AM logic, a specific optimization of the global logic, and possibly implement a 3D silicon device to increase the available area. Frascati and Milano worked on the design of the full custom AM cell. This work is the critical element of this project because advanced techniques are required to meet the density and power consumption goals. This element will require intensive simulation to verify functionality under all conditions.

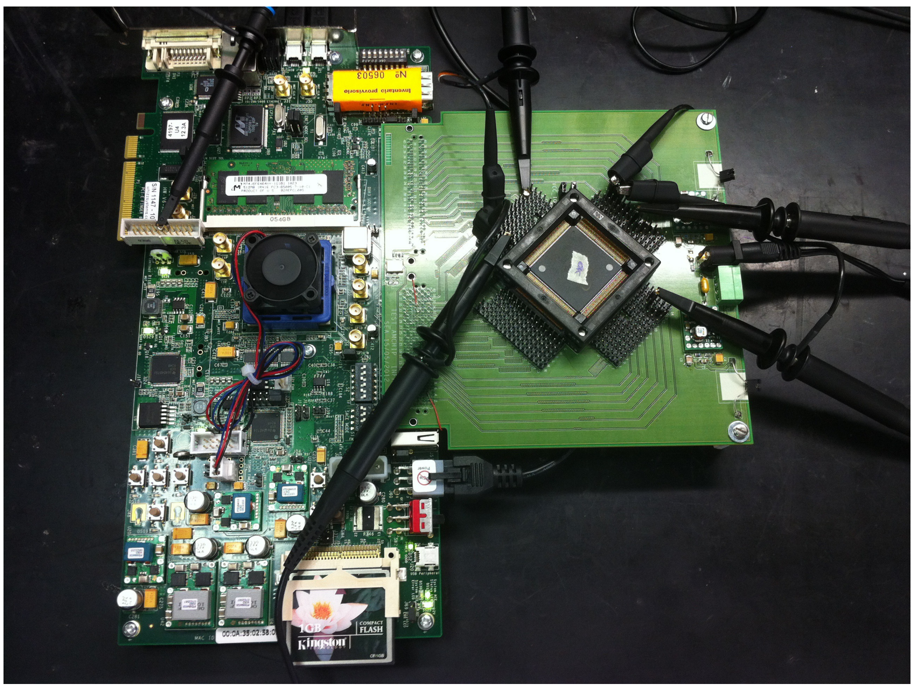

Figure 14: Test system for the AMChip04.

Hundred prototype AMchip04 were produced and delivered at the end of May. Figure 14 shows the test system setup that uses a Xilinx ML605 evaluation board in combination with a PCB that mounts one AMchip04 prototype in a ZIF socket. The Virtex FPGA on the ML605 board is programmed to implement a microblaze processor that runs linux in order to execute the test progam directly on the ML605 board. The test program receives the test vectors via ethernet and send them to the AMchip comparing the output on a clock by clock basis. The AMchip04 prototype perform as expected with a perfect match of predicted output versus expected output. The AMchip04 has been tested up to 100MHz. In particular the full custom AM cell is performing as expected. During the tests we measured the power consumption and found that it was higher than the expected value but still within the worst case expected values. We studied the different contributions to the power consumption that are reported in Table 3.
The estimated power for the full custom AM cell was of 60mA. The measured increased in power consuption is acceptable. The power consumption of other contributions was expected to be significantly smaller. The new version of the device will reduce power consumption by lowering the core voltage to 1.0V using specific cells and exploring the use of low-Vt transitor that allow a reduction of dinamic power consuption in exchange for a higher leakage current.

contributor	current drawn (mA)
leakage	7
clock distribution	30
receiving input	6
data distribution	82
full custom AM cell	70
total	195

Table 3: Core current draw by the AMchip04 split into different contribution. The current is evaluated at 100MHz at the nominal input core voltage of 1.2V.

The Frascati group led the FTK vertical slice integration at CERN. During 2011 a vertical slice has been assebled at CERN. A first setup, see Figure 15 has been assebled in TDAQ lab 32 with a VME crate, an Associative Memory board (AMB), and an EDRO board with one FTK_IM installed. With this setup data flow has been established sending data over SLink using a QUEST card. In September the system has been moved to USA15 cavern where it has been connected to the SCT detector and ATLAS DAQ. During Setember-October the system has been intgrated in the ATLAS DAQ and dataflow was established with level-1 rate up to 70kHz. Work continued to prepare a realist pattern bank to be loaded in the hardware and decoding of input data. New software and firmware has been deployed. The updated system has been commissioned at the begining of 2012. It has been included in the ATLAS data taking for a few days, for Cosmics runs first and then during pp collisions at 2.76 TeV. With collisions data FTK found the first pattern-match. The FTK vertical slice activity will continue during the 2013-2014 shutdown. Since TDAQ lab 32 has been dismissed a new FTK setup is being prepared in TDAQ lab 4 for this purpose.
Guido Volpi coordinated the simulation activity of the Fast-Tracker collaboration. The simulation activity was essential to define the specifications for the AMchip design, including the variable resolution presented at the ANIMMA 2011 conference. It was essential to find an affordable configuration for FTK at high luminosity $3*10^{34}$ and 10^{35} cm^{-2}s^{-1}. The proof-of-principle was then integrated into the current FTKSim package. A new and important branch of activity emerged: the integration of the standalone FTK simulation within the ATLAS software and production frameworks. we worked in close contact with the ATLAS experts at CERN and this new activity is now half completed. This is already beyond the needed schedule because the FTK studies for the Technical Design Report can be completed with the standalone simulation, but it will allow a wider application of the FTK simulation inside the Atlas collaboration.

6 The new Small Wheel upgrade

The upgrade program for LHC is under study with the aim to increase the luminosity by a factor of 10. The present detectors of ATLAS have been designed according to the rates expected at the nominal LHC luminosity. Fig. 1 shows the expected counting rates in the ATLAS Muon chambers. With the luminosity upgrade of LHC, the rate of prompt muons and the background of photons and neutrons will increase proportionally. In these conditions, an upgrade of the present muon chambers in the End-cap inner and middle muon wheels, the latter for rapidity $\eta > 2$, will be needed. For their replacement, muon chambers based on the Micromegas technology that com- bine precision measurement and triggering capability in the same detector have been chosen for precision tracking and eventually for triggering. The final chambers to be used for the upgrade of the ATLAS Muon Spectrometer should be of approximate size 1 m x 2 m, with the following characteristics:

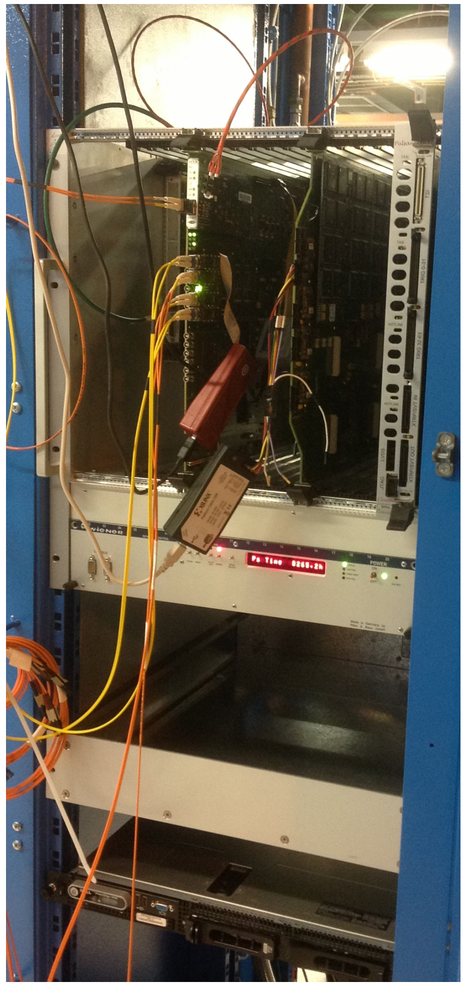

Figure 15: FTK vertical slice in USA15.

- high-rate capability ($>$5kHz=cm^2);
- spatial resolution $\sim$100mm for impact angles 45;
- transverse coordinate resolution $\sim$1 cm;
- time resolution: $\sim$ 5-10 ns;
- high efficiency >98%;
- level-1 triggering capability;
- radiation hardness and good ageing properties.

The New Small Wheel is a first priority project for the ATLAS experiment to maintain and improve the trigger and the excellent tracking performance of the end cap muon system at the highest energy and lu-minosity expected. Our lab has been chosen as one of the production sites. First assembling tests are ongoing. Extensive tests have been performed on prototypes with cosmics and at test beams.

6.1 Cosmic Ray Stand

The ATLAS cosmic Ray Stand (CRS) is located in the Gran Sasso hall at LNF. It was originally designed for the test of the ATLAS muon chambers (MDT). A recent picture is shown on the left panel of figure 16. A fully instrumented MDT chamber is hooked to a couple of rails that allow it to roll in and out. Plastic scintillators are used for triggering: three pairs are mounted on top of the MDT chamber; three pairs are placed on ground, below 30 cm of iron used for screening from low-momentum muons. The CRS setup has been recently revised in view of the future tests of the MicroMegas chambers. The MDT chamber will be moved to the upper rails and in its place we will put a table where we will lay the chambers under test. The table will be free to roll on the rails to easy the detector posistioning (right panel of figure 16). The trigger scintillators will also be re-arranged.

Figure 16: Left: Recent picture of the ATLAS CRS. The top scintillators used for the trigger are visible, and also two MDT chambers, one of which is fully instrumented. Right: A sketch of the new CRS setup. The instrumented MDT chamber is moved to the upper rails and in its place is a table upon which detectors under test will be placed. The table is able to roll on the rails to easy the positioning of detectors.

In order to test the MicroMegas we will use as a reference tracker the MDT chamber. It is designed to have a position resolution of about 70 μm. During this year we put back to work the trigger, acquisition, and gas systems. Writing of a new reconstruction package is underway. A first example of reconstructed cosmic tracks is shown in figure 17.

7 MicorMegas tests with particle beams

A number of tests on MicroMegas have been carried out at beam test facilities (BTF) at CERN and LNF. Tests at CERN were performed at H2 and H6 beam lines at the Super Proton Synchrotron (SPS), providing 120 GeV/c pion beam with an intensity ranging from 5 to 30 kHz over an area of 2 cm^2. During the H2 test beam data was taken in presence of a magnetic field of intensity up to 0.5 T. Several prototype chambers were tested. These had an active area of about 10$\times$10 cm^2 and strip pitches ranging from 250 to 400 μm. A gas mixture of 93% Ar and 7%CO_2 was used. The chambers were mounted on a frame as shown in figure 18 left. They were free to rotate around the vertical axis allowing the test of the tracking capabilities for non orthogonal tracks (μTPC mode). The readout was performed with an APV25 hybrid chip sampling the integrated charge on the strips every 25 ns. An example of APV25 charge samplings is shown in figure **??** right. Here the spectrum is fit with a function taking into account the charge collection and induction on the strips and the APV25 signal response. Typical duration of the signal is

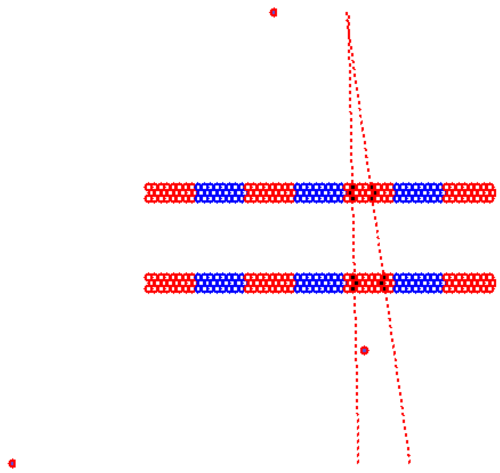

Figure 17: Tracks of two simultaneous cosmic rays reconstructed in the MDT chamber.

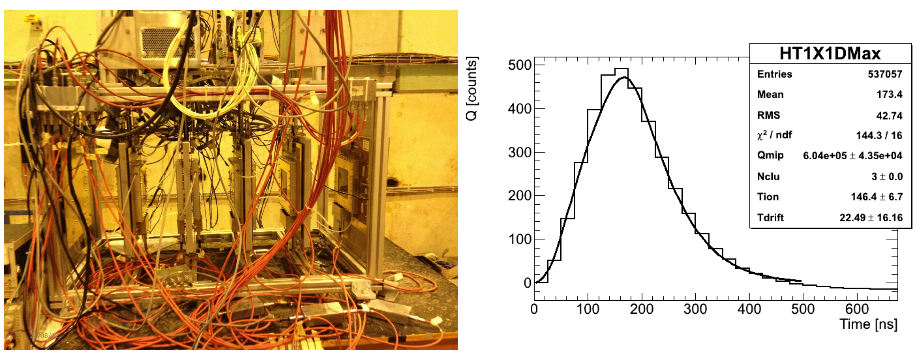

Figure 18: left: picture of the test beam setup at H6 beam line at CERN SPS; right: charge samplings measured from the APV chip.

about 100-200 ns compatible with the ion drift-time. The exponential decay-time of the signal is due to an RC-CR shaper with a 50 ns time-constant. These prototypes showed an efficiency close to 100% and spatial resolution of about 100μm both for orthogonal and diagonal tracks.
Test with electron were performed at the Frascati BTF with momenta of about 500 MeV/c 20 Hz rate over an area of about 2 cm^2. Three 10x10 cm2 MM chambers have been exposed to 0.5 GeV BTF electron beam. The experimental setup is shown in figure 19. Fig 1: Picture of the experimental setup. It consists of 2 scintillator counters providing the trigger, three 10x10 cm2 MM chambers, and a lead-scintillating fibers calorimeter to monitor the spill multiplicity. MMs are filled with a 93% Ar 7% CO2 gas mixture and are operated with a drift field of 0.6KV per cm and a gap of 540 V. Two MMs have been readout with APV25 and one MM has been readout with a low noise current to voltage amplifier prototype. High gain, 220K, has been achieved with 3 stages allowing a good output dynamics (1V) and a small power consumption(75mV). To increase the detector readout area, at the price of an increase of the MM output capacity, four X strips with 125 m pitch have been connected in parallel. Typical signals of 200/300 mV with

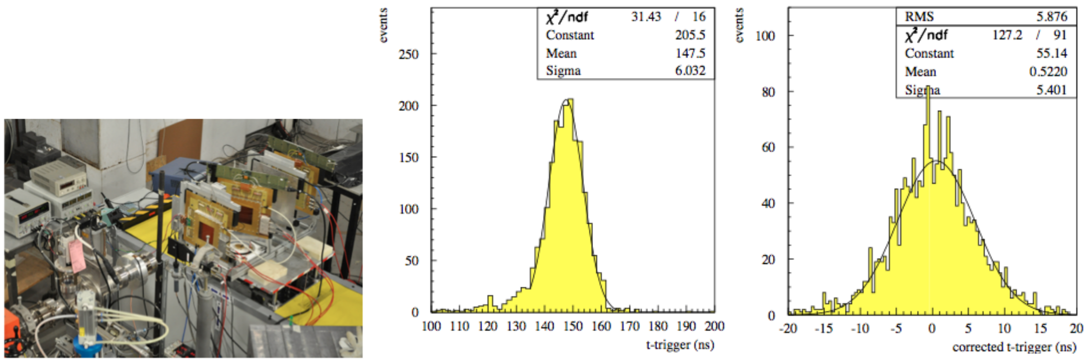

Figure 19: right: experimental setup at BTF; t-trigger distribution:uncorrected (center) and corrected (right) for the collected charge value

about 100 ns width have been observed in coincidence with the trigger. The analogic signal has been discriminated with 75 mV threshold. Time and time over threshold information are provided by a multi-hit TDC. The t-trigger distribution, the difference in time between the discriminated signal and the triggershows a time resolution of about 6 ns. The small tail at low t-trigger values is due to events with low collected charge. Figure **??** right shows the t-trigger distribution after the charge effect correction.

Public presentations:

- SM@LHC2012 10-Apr-12 LHC MPI and underlying event results (ATLAS+CMS)
- Search for the SM Higgs boson in the HWW(*)ll decay channel at LHC, LNF mini-workshop 28th March 2012
- M Antonelli "discovery of a narrow resonance with at 125 GeV at LHC", Los Alamos general Seminar.
- "A Hardware Track Finder for the ATLAS Trigger" presented at Real Time 2012 Conference 13/6/2012
- "A Fast Hardware Tracker for the ATLAS Trigger System" (Poster) presented at Frontier Detector for Frontier Physics 21/6/2012
- "ARAMIS: Advanced Real-time Architectures of Data processing, Pattern Recognition and Data Transmission for Frontier Applications in High Energy Physics, High Reliability Systems and Visual Science" (Poster) presented at Frontier Detector for Frontier Physics 21/6/2012

Publications:

- "Search for the Standard Model Higgs boson in the H-¿WW(*)-¿ lnulnu decay mode with 4.7 fb-1 of ATLAS data at sqrt(s) = 7 TeV" ATLAS-CONF-2012-012, 5 March 2012
- "Search for the Standard Model Higgs boson in the H-¿WW(*)-¿lvlv decay mode using Multivariate Techniques with 4.7 fb-1 of ATLAS data at sqrts=7 TeV" ATLAS-CONF-2012-060, 6 June 2012

- Observation of an Excess of Events in the Search for the Standard Model Higgs Boson in the H -¿ WW -¿ l nu l nu Channel with the ATLAS Detector” ATLAS-CONF-2012-098, 18 July 2012
- ”Update of the H -¿ WW(*) -¿ e nu mu nu analysis with 13.0 fb1 of sqrts = 8 TeV data collected with the ATLAS detector” ATLAS-CONF-2012-158, 13 November 2012
- ”Measurements of the properties of the Higgs-like boson in the four lepton decay channel with the ATLAS detector using 25 fb-1 of proton-proton collision data”, ATLAS-CONF-2013-013
- ”Updated results and measurements of properties of the new Higgs-like particle in the four lepton decay channel with the ATLAS detector”. ATLAS-CONF-2012-169
- ”Observation of an excess of events in the search for the Standard Model Higgs boson in the H-¿ ZZ(*)-¿ 4l channel with the ATLAS detector”, ATLAS-CONF-2012-092
- ”Observation of a new particle in the search for the Standard Model Higgs boson with the ATLAS detector at the LHC”, Phys.Lett. B716 (2012) 1-29
- ”Observation of a new particle in the search for the Standard Model Higgs boson in the H ZZ()4 channel and its properties using 4.6 fb1 and 20.7 fb1 of proton-proton collisions at s = 7 TeV and 8 TeV, respectively, recorded with the ATLAS detector.”,ATL-COM-PHYS-2013-146
- ”Observation of a new particle in the search for the Standard Model Higgs boson in the H ZZ()4 channel : limits on the for VBF and VH production of the new particle and High mass search using 4.6 fb1 and 20.7 fb1 of proton-proton collisions at s = 7 TeV and 8 TeV, respectively, recorded with the ATLAS detector.”ATL-COM-PHYS-2013-145
- ”Observation of a new particle in the search for the Standard Model Higgs boson in the H ZZ()4 channel : mass and signal strength measurement using 4.6 fb1 and 20.7 fb1 of proton-proton collisions at s = 7 TeV and 8 TeV, respectively, recorded with the ATLAS detector.”ATL-COM-PHYS-2013-144
- ”Observation of a new particle in the search for the Standard Model Higgs boson in the H ZZ()4 channel and measurements of its properties using 4.6 fb1 and 13.0 fb1 of proton-proton collisions at s = 7 TeV and 8 TeV, respectively, recorded with the ATLAS detector.” ATL-COM-PHYS-2012-1483
- ”Search for the Standard Model Higgs boson in the decay channel HZZ()4 with 5.8 fb1 of pp collision data at s=8 TeV with ATLAS”, ATL-COM-PHYS-2012-835
- R. Di Nardo et al., Enabling data analysis la PROOF on the Italian ATLAS Tier-2s using PoD, J. Phys.: Conf. Ser. 396 (2012) 032043, [http://iopscience.iop.org/1742-6596/396/3/032043/]
- The EDRO board connected to the Associative Memory: a ”Baby” FastTracker processor for the ATLAS experiment https://cdsweb.cern.ch/record/1382040/, doi:10.1016/j.phpro.2012.02.502, Physics Procedia, Vol 37, 2012, 1772-1780, ISSN 1875-3892
- The FastTrack Real Time Processor and Its Impact on Muon Isolation, Tau and b-Jet Online Selections at ATLAS, IEEE Trans. Nu cl. Sci. 59, 348. http://dx.doi.org/10.1109/TNS.2011.2179670

- “Associative Memory for L1 Track Triggering in LHC Environment”, Real Time Conference (RT), 2012 18th IEEE-NPSS , vol., no., pp.1-6, 9-15 June 2012, doi: 10.1109/RTC.2012.6418193

- The AMchip04 and the processing unit prototype for the FastTracker, 2012 JINST 7 C08007

References

1. ATLAS Collaboration, “Performance of missing transverse momentum reconstruction in proton-proton collisions at 7 TeV with ATLAS”, EPJC 72 (2012), arXiv:1108.5602 [hep-ex]

2. M.Cacciari and G.P.Salam, “PileUp subtraction using jet areas”,Phys.Lett.B659 (2008) 119-126, arXiv:0707.1378 [hep-ph]

3. ATLAS Collaboration, “Measurements of the properties of the Higgs-like boson in the $W \to l\nu l\nu$ decay channel with the ATLAS detector using 25 fb^{-}1 of proton-proton collision data”, ATLAS-CONF-2013-030

4. : D. Barberis et al., ”ATLAS computing activities and developments in the Italian Grid Cloud”, J. Phys.: Conf. Ser. 396 (2012) 042052

5. : R. Di Nardo et al., Enabling data analysis la PROOF on the Italian ATLAS Tier-2s using PoD, J. Phys.: Conf. Ser. 396 (2012) 032043, [http://iopscience.iop.org/1742-6596/396/3/032043/]